https://doi.org/10.5194/egusphere-2026-6583
Preprint. Discussion started: 17 November 2026
© Author(s) 2026. CC BY 4.0 License.

Surface flux contributions to Mediterranean heatwaves: a new Lagrangian diagnostic

Vinita Deshmukh[1], Andreas Stohl[1], and Marina Dütsch[1]
[1]Institut für Meteorologie und Geophysik, Universität Wien, Wien, Österreich
Correspondence: Vinita Deshmukh (vinita.deshmukh@univie.ac.at)

Abstract. The increasing frequency of Mediterranean heatwaves is associated with widespread impacts on human health, agriculture, and infrastructure. Previous studies point out that the intensity of heatwaves depends not only on the advection of heat and moisture into the region but also on the heat and moisture supplied by turbulent surface fluxes to the advected air mass, yet the contribution of these fluxes remains difficult to quantify. Here, a Lagrangian framework is developed that couples surface sensible and latent heat fluxes from ERA5 directly to the advected air mass, through the near-surface source–receptor relationship of the FLEXPART particle dispersion model, and reconstructs the moist static energy (MSE) of the air arriving in the heatwave region as the sum of its advected initial condition and the surface-flux contribution accumulated along the pathway. The approach is analogous to well-established methods coupling surface greenhouse-gas fluxes to atmospheric concentrations, is fully quantitative, and requires no subjective thresholds or inference of changes along individual trajectories. Applied to heatwaves occurring over Greece in seven years between 1982 and 2025, the reconstruction skillfully reproduces the day-to-day variability of the MSE in the heatwave region in every event ($r = 0.85$–0.94), with a positive bias consistent with the fact that our framework currently neglects radiative cooling of the air. Using 10-day backward calculations, the variability of MSE at the receptor (region of the heatwave) is caused mainly by variability in the air mass initial conditions, i.e. the MSE of the air mass 10 days upstream. We also tracked the air on all other summer days during the seven years and found that the extra energy on heatwave days is mainly due to anomalously large initial potential energy, sometimes supplemented by anomalously high enthalpy. An important finding is that the surface fluxes actually reduce the initial anomaly of heatwave days compared to other summer days,contrary to previous studies emphasizing the role of land-atmosphere interactions for heat waves. While the sensible heat fluxes are sometimes enhanced, the latent heat fluxes are strongly reduced in all heatwave cases compared to the other summer days. The lower latent heating is consistent with the role of soil moisture found in earlier studies. In most heatwave cases, the largest flux contribution to the MSE comes from dry continental surfaces such as North Africa and Greece itself, which explains why latent heat fluxes are smaller than on other summer days. Our new framework provides a direct and physically consistent way to attribute the moist static energy of a heatwave to advection and to surface fluxes, resolved by region and by flux type (latent or sensible). It is generally applicable to any receptor region and any weather event, and is also suitable for climatological studies.

https://doi.org/10.5194/egusphere-2026-6583
Preprint. Discussion started: 17 November 2026
© Author(s) 2026. CC BY 4.0 License.

1 Introduction

Heatwaves are becoming more frequent, intense, and persistent under climate change, with strong impacts on human health, agriculture, and wildfire risk (Perkins, 2015; Kautz et al., 2022). Heat-related mortality has risen sharply in recent decades: heat-related deaths in Europe and North America have increased by about 30 % over the past two decades (WMO, 2023), and the number of days with strong heat stress in Europe continues to rise (Vautard et al., 2023). The Mediterranean region in particular is warming at roughly 1.5 times the global average rate (Lelieveld et al., 2012; Zittis et al., 2021), leaving the continental region particularly exposed during the summer. Lagrangian studies of heatwaves have so far mostly focused on western and central Europe (Zschenderlein et al., 2019) or on global composites (Röthlisberger and Papritz, 2023), while the eastern Mediterranean has received comparatively little attention. Greece has experienced some of the most severe of these events, such as the 1987 Athens heatwave (Katsouyanni et al., 1988) and the exceptional summer of 2007 (Founda and Giannakopoulos, 2009). Hence it is important to understand the processes and mechanisms associated with heatwaves occurring over this region. It is very well known that large-scale atmospheric conditions such as anticyclonic blocking and subtropical ridges (Stefanon et al., 2012) trigger Mediterranean heatwaves, which are associated with atmospheric processes such as subsidence and adiabatic warming (Kuglitsch et al., 2010) but also cause stagnant conditions enhancing local land-atmosphere interactions involving soil moisture deficits. These soil moisture deficits can be intensified further by persistent blocking circulations, which act as slow drivers sustaining and amplifying heatwave conditions (Fischer et al., 2007; Stefanon et al., 2012). Furthermore, heatwaves exacerbated by low soil moisture can lead to other extreme events such as wildfires and droughts (Witte et al., 2011; Davini et al., 2017; Miralles et al., 2014). The relative importance of these processes differs between events. Heatwaves can be driven by local processes, such as clear-sky subsidence, or can be sustained by the advection of warm air from remote continental regions (Fildier et al., 2023b). Quantifying the relative roles of local subsidence, local surface heating and remote contributions requires identifying where the heatwave air mass originates and how its thermodynamic state, heat and moisture content of the airmass evolve along the way. Lagrangian diagnosis is well suited to this, as it can follow an air mass and the thermodynamic modifications it undergoes between its origin and the heatwave region (Zschenderlein et al., 2019). Sodemann et al. (2008) introduced a moisture source algorithm in which moisture uptakes within the atmospheric boundary layer (ABL) are inferred from the change in specific humidity along the trajectories, and their contribution to precipitation in the target region is quantified using a discounting method that accounts for precipitation occurring en route. This approach has been applied extensively to moisture sources for hydrological extremes such as heavy precipitation and drought. For heatwaves, a similar approach infers heat sources from changes in the parcel's dry static energy within the ABL (Schumacher et al., 2019). These trajectory-based methods have proven valuable, but they are highly sensitive to heat or moisture fluctuations along the trajectories, some of which are not related to actual heat or moisture uptakes. Such fluctuations can be caused by interpolation errors, turbulent motions, or the temporal discontinuities in the driving meteorological data caused by data assimilation. In fact, for these reasons a clear separation between evaporation and precipitation along the trajectories is not possible (Stohl and James, 2004), and the same applies to heat losses and gains. To reduce the impact of these artifacts, Sodemann et al. (2008) introduced thresholds, for instance, a minimum specific-humidity increase to identify a moisture source. The uncertainties in

https://doi.org/10.5194/egusphere-2026-6583
Preprint. Discussion started: 17 November 2026
© Author(s) 2026. CC BY 4.0 License.

these approach are sensitive to these thresholds and also the time intervals over which heat and moisture gains and losses are diagnosed. These combined uncertainties highlight a need for an alternative approach to diagnose the contribution of surface fluxes, as well as their location and type, to form a heatwave airmass.

This study provides a novel alternative approach by coupling surface turbulent fluxes from a meteorological reanalysis directly to the air mass that encounters them. It is inspired by methods used to quantify the contribution of greenhouse gas surface fluxes to atmospheric concentrations, for which Lagrangian models have long been used (Stohl et al., 2009; Say et al., 2016). This new method is fully quantitative, independent of subjective criteria, can cleanly separate heat (and moisture) gains and losses by surface fluxes, and can map out their contributions to the heat (or moisture) content of an air mass in space and time.

In this study the approach is demonstrated at the example of Mediterranean heatwaves, where a framework is established expressing the moist static energy of the air arriving over the heatwave region as the sum of two terms: the energy the air mass already carried at the start of its ten-day pathway, and the energy it acquired from surface fluxes along the way. Two aspects are addressed here. The first is whether the new framework can reproduce the day-to-day variability of moist static energy in the heatwave region. Once this is established, the flux term is decomposed to quantify the sensible and latent heat flux contributions and to identify the regions from which they originate. The framework is therefore first demonstrated in detail for a single heatwave over Greece, then applied to 12 other events between 1979 and 2025, this is done to identify the dominant source regions and the relative sensible and latent heating contributions for heatwaves occurring specifically over Greece.

2 Data and Methodology

2.1 Data

All atmospheric fields used in this study are taken from the ERA5 reanalysis (Hersbach et al., 2020) at $0.5° \times 0.5°$ horizontal resolution. Heatwave detection uses daily maximum 2 metre temperature ($T_{\max}$) for the period 1979–2025, and the Lagrangian transport simulations are driven by hourly wind fields at the same resolution.

2.2 Heatwave detection

According to the World Meteorological Organisation (WMO), heatwaves are defined as periods during which the daily maximum temperature exceeds the long-term mean temperature by a certain degree, based on the specific location and time of year, for consecutive days. Various studies use different definitions of heatwaves. Heatwaves are detected over a Greece-centred domain (blue box in Figure 1, 34–42.5°N, 19–27°E), restricted to the summer months of June, July, and August (JJA). The detection algorithm proceeds as follows:

1. Climatological threshold: local 95th percentile of daily $T_{\max}$ computed over a $\pm$10-day window centred on each calendar day for the 1991–2025 reference period.

https://doi.org/10.5194/egusphere-2026-6583
Preprint. Discussion started: 17 November 2026
© Author(s) 2026. CC BY 4.0 License.

Table 1. Summary of detected heatwave events over the Greece-centred domain. HW days is the total number of detected heatwave days in that summer; Episodes is the number of separate heatwave periods; Peak day is the date of maximum temperature anomaly. $T_{\max}$ and T anomaly is the average temperature anomaly over all detected heatwave days of each year.

Year	HW days	Episodes	Peak day	$T_{\max}$ (°C)	T anomaly (°C)
1982	5	1	1982-06-25	44.6	6.4
1987	8	1	1987-07-26	43.1	4.0
1988	5	1	1988-07-07	43.3	7.4
2007	18	2	2007-06-26	46.2	7.9
2021	10	2	2021-06-25	40.5	4.7
2024	21	3	2024-08-14	40.5	4.9
2025	12	2	2025-07-25	41.8	5.5

2. Spatial coherence: a grid cell is classified as hot if $\geq 60\%$ of the surrounding $2° \times 2°$ land area simultaneously exceeds the climatological threshold.

3. Temporal persistence: spatially coherent hot regions are tracked in time, and events are retained only if they persist for ≥ 5 consecutive days.

4. Event merging: fragmented events separated by ≤ 2 days and spatially proximate, with centroid distance $< 6°$, are merged into a single episode.

Using this method, 12 strong and persistent heatwaves were identified over 43 years (see table 1). Some years include more than one heatwave episode. These cases are also consistent with documented heatwave events over Greece and with previous studies (Founda et al., 2022). The 2007 event stands out as one of the most intense heatwaves, with the temperature record of 46.2°C and the largest temperature anomaly of 7.9°C. A detailed analysis to demonstrate the framework is carried out for this year.

2.3 A Lagrangian surface-flux framework for moist static energy

Heat and moisture are tightly coupled variables which are modified together by the surface turbulent fluxes of sensible and latent heat. They are best analysed jointly through a single moist thermodynamic variable, the moist static energy (MSE):

$$MSE = C_p T + L_v q + g z, \tag{1}$$

where $C_p = 1004.7$ J kg^{-1} K^{-1} is the specific heat capacity of dry air at constant pressure, T is absolute air temperature, $L_v = 2.2 \times 10^6$ J kg^{-1} is the latent heat of vaporisation, q is specific humidity, $g = 9.81$ m s^{-2} is the gravitational acceleration, and z is the geopotential height above sea level. MSE is conserved under both dry and moist adiabatic processes (Emanuel and Živković Rothman, 1999), so that phase changes redistribute energy between the sensible and latent heat terms without

https://doi.org/10.5194/egusphere-2026-6583
Preprint. Discussion started: 17 November 2026
© Author(s) 2026. CC BY 4.0 License.

changing MSE. The sensible heat term C_pT is modified by the surface sensible heat flux (SSHF). The latent heat term L_vq is modified by the surface latent heat flux (SLHF). Furthermore, condensation and evaporation of moisture convert sensible heat to latent heat and vice versa. The geopotential term gz carries no direct surface-flux contribution but changes as the air mass ascends or descends.

The idea of our new framework is that the MSE of the air mass arriving at the receptor (region of interest), can be reconstructed as ($MSE_{\mathrm{rec}}^{\mathrm{recon}}$) the sum of two contributions: initial conditions, the MSE it already carried at the start of its ten-day pathway, denoted MSE_{IC}, and the MSE it gained from surface sensible and latent heat fluxes along the way, denoted $\Delta MSE_{\mathrm{flux}}$, here IC and $flux$ stands for initial conditions and flux contribution. Thus,

$$MSE_{\mathrm{rec}}^{\mathrm{recon}} = MSE_{\mathrm{IC}} + \Delta MSE_{\mathrm{flux}}. \tag{2}$$

As MSE is conserved under adiabatic vertical motion, the geopotential term is represented in both MSE_{IC} (as $g\,z_{\mathrm{IC}}$) and the receptor value (as $g\,z_{\mathrm{rec}}$): as the air mass descends, potential energy is converted adiabatically into sensible heat within the same conserved quantity, so the net effect of subsidence is already captured in the difference between MSE_{IC} and MSE_{rec}, and no separate subsidence term is added to Eq. (2).

Evaluating MSE_{IC} and $\Delta MSE_{\mathrm{flux}}$ requires knowing where the air mass originated and which surfaces fluxes it encountered along its pathway. This is obtained by utilising the Lagrangian particle dispersion model FLEXPART, and by the source–receptor relation (SRR) and initial-condition sensitivity field it produces, described in the next Section 2.4.

2.4 FLEXPART model setup and the source–receptor relation

Air-mass transport is simulated with the Lagrangian particle dispersion model FLEXPART version 11.0 (Bakels et al., 2024), run globally with an output resolution of $0.5°$ and driven by hourly ERA5 meteorological fields (Hersbach et al., 2020) of $0.5°$ resolution. The model is run in backward mode with 900 s synchronisation and sampling steps.

Trajectories are followed backwards for 10 days. This length is chosen because it corresponds to the average atmospheric residence time of water vapour (Läderach and Sodemann, 2016), and it is a period over which radiative cooling in the free atmosphere is not expected to dominate the energy budget, at least in cloud-free conditions. Radiative fluxes are not available as 3-D fields in ERA5 and are therefore not included in the process attribution.

Releases are made five times per day (06, 09, 12, 15 and 18 UTC) on every day from 1 June to 31 August, giving 460 releases for each heatwave event year. On each day, particles are released from all land grid cells within the Greece domain (34–42.5°N, 19–27°E; blue box in Figure 1). Trajectories are initiated with 500 particles released per land grid cell at 50 m above the surface, the height taken to represent the near-surface mixed layer. The Emanuel convective scheme (Emanuel and Živković Rothman, 1999) and a boundary-layer turbulence scheme represent sub-grid-scale mixing processes. Releasing air masses on every summer day, rather than only on heatwave days, covers the full range of receptor MSE, from ordinary summer days to heatwave peaks, and provides a continuous time series for testing the budget closure of each event.

Each release is labelled as a heatwave or summer-day release. Releases made on days that satisfy all the heatwave criteria (from Section 2.2) are labelled heatwave releases, and all remaining releases are labelled summer-day releases. Releasing air

https://doi.org/10.5194/egusphere-2026-6583
Preprint. Discussion started: 17 November 2026
© Author(s) 2026. CC BY 4.0 License.

masses throughout the whole summer therefore provides not only a continuous time series for the closure test, but also a large set of ordinary summer-day releases which serve as a reference, against which the airmass transport and the energy that heatwave air masses carry ten days before arrival can be compared.

For each release, FLEXPART produces two sensitivity fields. The source–receptor relation (SRR), introduced by Stohl et al. (2003) and formalised by Seibert and Frank (2004), gives the residence time of the released particles in each grid cell along their backward pathway, and thereby the sensitivity of the receptor to surface fluxes in these cells. Since only surface fluxes are of interest here, the SRR is written out only for the lowest model layer, 0–100 m above the ground, at $1^\circ \times 1^\circ$ horizontal and hourly temporal resolution. The spatial distribution of the SRR, integrated over all heatwave day releases during the 2007 heatwave period, is shown in Figure 2a. The second FLEXPART output for each release is the three-dimensional gridded spatial distribution of the tracked airmass at its termination points, which represents the sensitivity of the receptor MSE to the MSE ten days upstream, i.e., the initial conditions. Coupling this three-dimensional sensitivity field with the MSE computed from ERA5 gives the initial thermodynamic state of the air mass ten days upstream.

2.5 Reconstruction equations

With the SRR and initial-condition fields defined, the two terms of Eq. (2) can now be written explicitly. The initial thermodynamic state is its MSE, MSE_{IC}, at the trajectories origin, 10 days upstream from the release. It is computed from the ERA5 temperature, specific humidity, and geopotential height, weighted by the initial-condition sensitivity field:

$$MSE_{\mathrm{IC}} = \sum_{x=1}^{X}\sum_{y=1}^{Y}\sum_{z=1}^{Z} w_{x,y,z}\, MSE_{x,y,z}, \qquad \sum_{x=1}^{X}\sum_{y=1}^{Y}\sum_{z=1}^{Z} w_{x,y,z} = 1, \tag{3}$$

where $w_{x,y,z}$ is the FLEXPART sensitivity to the MSE large set of ordinary summer-day releases. These serve as a reference, against which the airmass transport and the energy that initial conditions in the model output grid box x, y, z, $MSE_{x,y,z} = (C_p T_{x,y,z} + L_v\, q_{x,y,z} + g\, z_{x,y,z})$ is MSE in grid box x, y, z taken from ERA5, and X, Y, Z are the number of FLEXPART output grid boxes in longitude, latitude and height coordinate directions.

The surface-flux contribution, $\Delta MSE_{\mathrm{flux}}$, is obtained by multiplying the hourly averaged SRR field by the corresponding hourly averaged ERA5 SSHF and SLHF fields of the same spatial resolution, and summing over all grid cells and time steps:

$$\Delta MSE_{\mathrm{flux}} = \sum_{x=1}^{X}\sum_{y=1}^{Y}\sum_{t=1}^{\tau} \frac{\mathrm{SRR}_{x,y,t} \times \mathrm{SSHF}_{x,y,t}}{\Delta z} + \sum_{x=1}^{X}\sum_{y=1}^{Y}\sum_{t=1}^{\tau} \frac{\mathrm{SRR}_{x,y,t} \times \mathrm{SLHF}_{x,y,t}}{\Delta z}, \qquad \Delta z = 100\ \mathrm{m}, \tag{4}$$

where $\tau = 240$ is the number of hourly time steps of the 10-day backward simulation, $\mathrm{SRR}_{x,y,t}$ is the sensitivity of the receptor MSE to energy volume fluxes into the lowest model layer of grid box x, y at time t, and $\mathrm{SSHF}_{x,y,t}$ and $\mathrm{SLHF}_{x,y,t}$ are the corresponding ERA5 surface sensible heat and surface latent heat fluxes in W m^{-2}. Division by the depth of the lowest model layer Δz is needed to convert the surface fluxes into volume fluxes into the lowest model layer.

The reconstructed (MSE $MSE_{\mathrm{rec}}^{\mathrm{recon}}$) is then compared with the computed MSE using ERA5 data ($MSE_{\mathrm{rec}}^{\mathrm{ERA5}}$). The two terms; $MSE_{\mathrm{rec}}^{\mathrm{recon}}$ and $MSE_{\mathrm{rec}}^{\mathrm{ERA5}}$ are not expected to agree exactly. Firstly, radiative heating and cooling in the atmosphere

https://doi.org/10.5194/egusphere-2026-6583
Preprint. Discussion started: 17 November 2026
© Author(s) 2026. CC BY 4.0 License.

is not included in the reconstruction. Under the clear-sky conditions typical of heatwaves, radiative cooling to space of order -1 K day^{-1} may be expected, so a positive residual $\varepsilon = MSE_{\mathrm{rec}}^{\mathrm{recon}} - MSE_{\mathrm{rec}}^{\mathrm{ERA5}}$ is anticipated. Secondly, the surface fluxes are prognostic model quantities that are not corrected by the 12-hourly data assimilation cycle used in ERA5 production, whereas MSE is affected by the data assimilation. Over a 10-day period, this can cause substantial differences between $MSE_{\mathrm{rec}}^{\mathrm{recon}}$ and $MSE_{\mathrm{rec}}^{\mathrm{ERA5}}$.

The agreement between $MSE_{\mathrm{rec}}^{\mathrm{ERA5}}$ and $MSE_{\mathrm{rec}}^{\mathrm{recon}}$ is assessed using the Pearson correlation coefficient r, the root-mean-square error, the slope of their linear regression, and the mean residual, which together characterise the systematic bias and its dependence on the magnitude of MSE, as well as random errors. This is discussed further in Section 3.1.

3 Application of the framework to heatwave events

In this study the framework is first demonstrated in detail for the 2007 Greek heatwave, the most intense event in the detection record (Table 1), for which each step of the reconstruction is shown explicitly (Section 3.1). It is then applied to all the detected events to quantify the source regions of the heatwave air masses and the regional distribution of the surface-flux contributions (Section 3.2).

3.1 The 2007 Greek heatwave- Case study

The 2007 summer in Greece comprised two detected heatwave episodes. The first, from 21 to 28 June, developed under a broad anticyclonic ridge over the central and western Mediterranean (Fig. 1a). By the peak of the episode, the ridge had intensified and shifted eastward over the Balkans and the eastern Mediterranean (Fig. 1b), the 2-metre temperature anomaly over Greece exceeded 7°C and the maximum temperature reached 46.2°C, while cool anomalies persisted over the North Atlantic. The second episode, from 18 to 26 July (Fig. 1c, d), recurred under a similar but slightly poleward-displaced blocking ridge. In both episodes the blocking configuration suppressed the westerly flow and directed air from North Africa toward Greece.

Fig. 2 shows the terms used to compute the flux contribution for the peak heatwave day (26-06-2007). The source–receptor relationship (Fig. 2a), i.e., the sensitivity to surface fluxes, shows where the air mass arriving in Greece (heatwave area within the blue box in Fig. 2) had surface contact during the preceding ten days. A broad near-surface transport pathway spanning North Africa, the Mediterranean, the Balkans, and parts of Western Europe can be seen. This pathway alone, however, only partly determines where the air mass acquired its heat and moisture. The ERA5 surface fluxes of sensible and latent heat, averaged over the 10 days of the Lagrangian particle tracking (Figure 2b,c) show that sensible heat flux was dominant over the dry land of North Africa and the Sahara, and latent heat flux was largest over the Mediterranean and the wetter continental surfaces to the north of the receptor region. The strongest latent heat fluxes are observed over the Gulf Stream due to strong air-sea interaction. The total heat flux contribution $\Delta MSE_{\mathrm{flux}}$ (see Eq. 4) during the 10-day tracking interval is obtained by multiplying the hourly SRR with the hourly sums of sensible and latent heat fluxes (shown in Fig 2d). Note that SRR values and heat fluxes are multiplied hour by hour during the tracking period, while Fig. 2 only shows the total SRR sensitivity and 10-day average fluxes. The flux contributions are largest where both SRR and heat fluxes are large at the same time: for example over

https://doi.org/10.5194/egusphere-2026-6583
Preprint. Discussion started: 17 November 2026
© Author(s) 2026. CC BY 4.0 License.

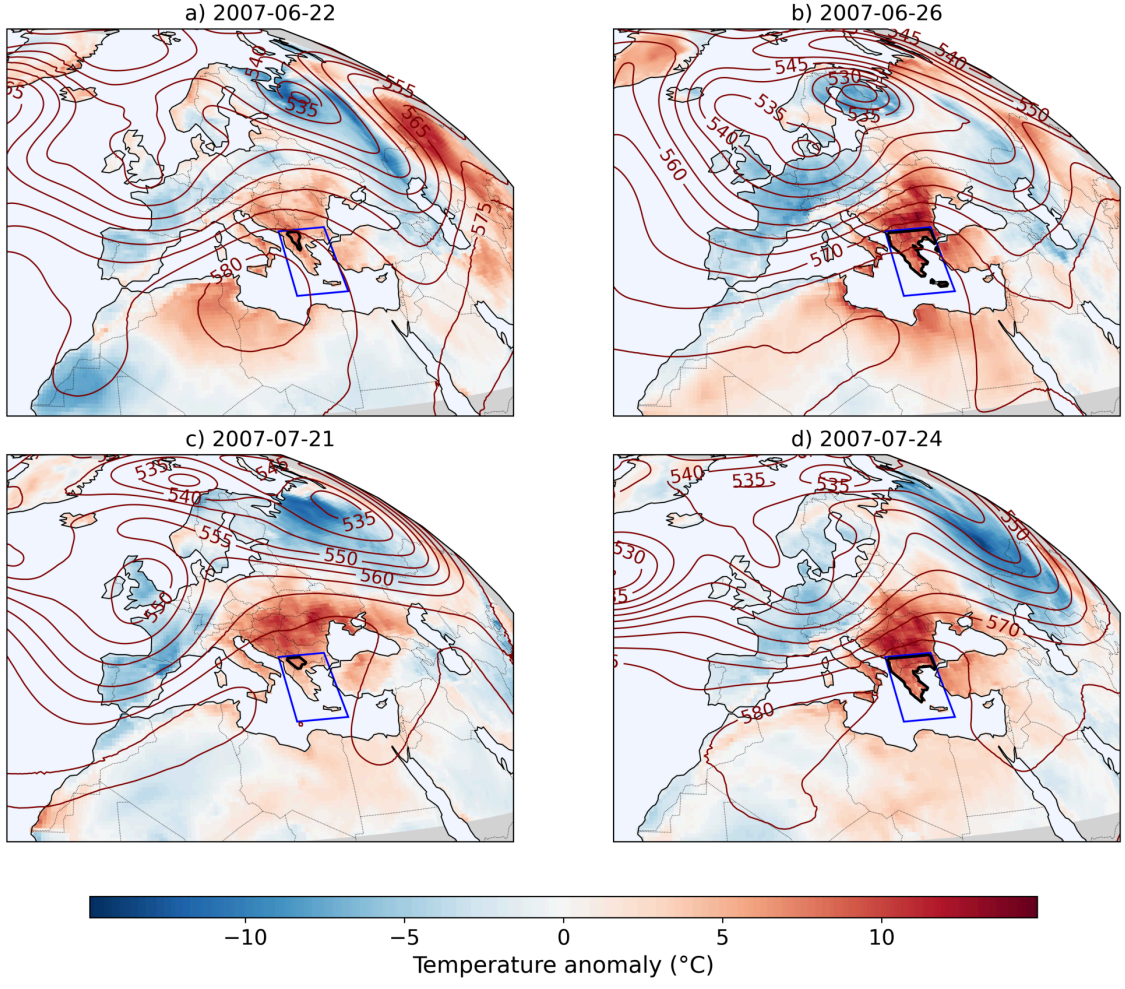


Figure 1. Synoptic overview of the 2007 Greek heatwave event. The thick black contour outlines the region where the heatwave was detected on that date, satisfying the criteria described in Section 2.2, and the Greece receptor domain is highlighted by the blue box (land areas in the region 34–42.5°N, 19–27°E). ERA5 500 hPa geopotential height contours are shown by dark maroon lines and are overlaid on 2-metre temperature anomalies in shading (°C) for four representative dates: (a) onset of the first episode, 22 June; (b) peak of the first episode, 26 June; (c) onset of the second episode, 21 July; and (d) peak of the second episode, 24 July.

https://doi.org/10.5194/egusphere-2026-6583
Preprint. Discussion started: 17 November 2026
© Author(s) 2026. CC BY 4.0 License.

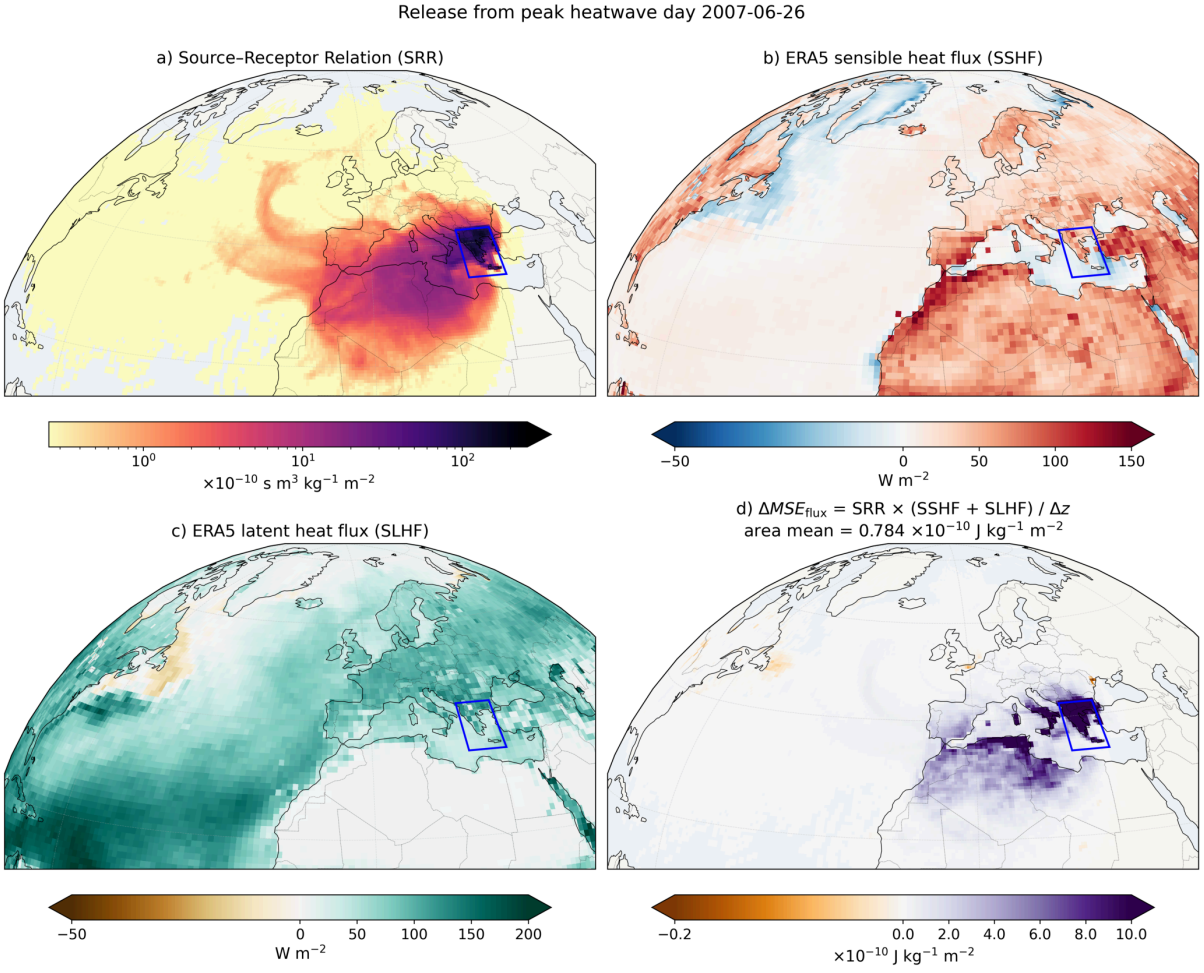


Figure 2. Spatial demonstration of framework. (a) Source–receptor relationship (SRR) integrated over 10 days back from the peak day of the 2007 heatwave. (b–c) ERA5 mean upward sensible (SSHF) and latent (SLHF) heat fluxes averaged over the 10-day period of particle backtracking. (d) Total surface-flux contribution per in J kg^{-1} m^{-2} (see eq. 4). The blue box marks the Greece receptor region.

https://doi.org/10.5194/egusphere-2026-6583
Preprint. Discussion started: 17 November 2026
© Author(s) 2026. CC BY 4.0 License.

the receptor region, North Africa, and western Europe such as as Italy and southern parts of Spain. In contrast, even latent heat large fluxes such as over the Gulf Stream do not contribute where the SRR values are small.

Having examined the surface-flux contribution in space and in time, the reconstruction is demonstrated as whole consisting of all three components of the equation (2) in Fig. 3. The vertically summed initial-condition MSE contribution MSE_{IC} (Fig. 3a) spans a large area, from the North Atlantic to much of Europe and North Africa, reflecting the broad distribution of particles after 10 days of backward tracking. Spatially summed, it gives the total initial-condition MSE contribution to the receptor region MSE. Total contributions from particles over the Atlantic, North Africa and North America are about 53%, 17.0% and 10%, respectively, while the receptor region itself contributes negligibly. The surface-flux contributions ΔMSE_{flux} (Fig 3b,c), by contrast, are far more confined and focussed on the receptor region, because they depend on the near-surface residence time, which peaks in the receptor region itself (see Fig. 2a). The initial energy the airmass carries is therefore arriving from remote and diffuse areas, whereas the energy it gains from the surface is more concentrated locally. The sensible heat flux contribution for this case (Fig 3b) is not uniformly positive. Over the Mediterranean and the Black Sea, where the advected air is warmer than the underlying water, the surface cools the air mass rather than heating it, giving a negative sensible heat flux contribution that partly offsets the heating over land. The latent heat flux contribution (Fig 3c) shows negligible negative values, as evaporation adds moisture almost everywhere along the pathway (only vapour condensation at the surface would lead to negative latent heat fluxes). While latent heat fluxes over the ocean are important, there is also large contributions from land surfaces, particularly over Italy and the receptor region itself.

Fig. 2d and Fig. 3 shows the flux contribution integrated over the full ten-day pathway spatially. The same contribution can also be followed in time, to see when along the pathway the air mass gains its energy. Fig. 4 shows the time series for the peak day of the 2007 heatwave, binned by days before release. Over most of the pathway, the air mass gains energy at a fairly steady rate of about 200-450 J kg^{-1} per day. The largest gain, however, comes at the very end, the last 12 hours alone add 37% of the total ten-day contribution of about 4550 J kg^{-1}, and the last 36 hours add almost half (47%). This behaviour is expected. The tracked near-surface air is in direct contact with the surface at the time of the release but surface contact decreases backward in time due to subsidence and vertical mixing. Thus, the SRR values are much smaller on earlier days than shortly before arrival in the target region. The type of heating also changes along the way. From two to ten days before release, sensible heating provides about 60–75 % of each daily contribution, consistent with the air mass travelling mainly over hot and dry land. In the final 36 hours, latent heating takes over and provides more than half of the contribution. In fact, nearly two-thirds of all latent heating is gained in this short period close to the receptor region. This shift towards latent heating is likely caused by the air mass crossing the open Mediterranean Sea shortly before reaching the receptor region, where evaporation is strong. Over the full ten days, sensible heating contributes 57 % (about 2600 J kg^{-1}) and latent heating 43 % (about 1950 J kg^{-1}).

Adding MSE_{IC} (Fig. 3a) and ΔMSE_{flux} (Fig. 2d) gives the reconstructed MSE MSE_{rec}^{recon}. Repeating this summation for every release through the study period gives a time series shown in Fig. 5a). The reconstructed MSE (maroon line in Fig 5a) is the sum of the initial condition (black dashed) and flux contributions (orange and blue shading). This maroon curve is quite well correlated to the MSE time series obtained directly from ERA5 at the receptor region at various releases (green line in Fig 5a). Both rise during the two heatwave episodes and fall during the break between them, and also the day-to-day

https://doi.org/10.5194/egusphere-2026-6583
Preprint. Discussion started: 17 November 2026
© Author(s) 2026. CC BY 4.0 License.

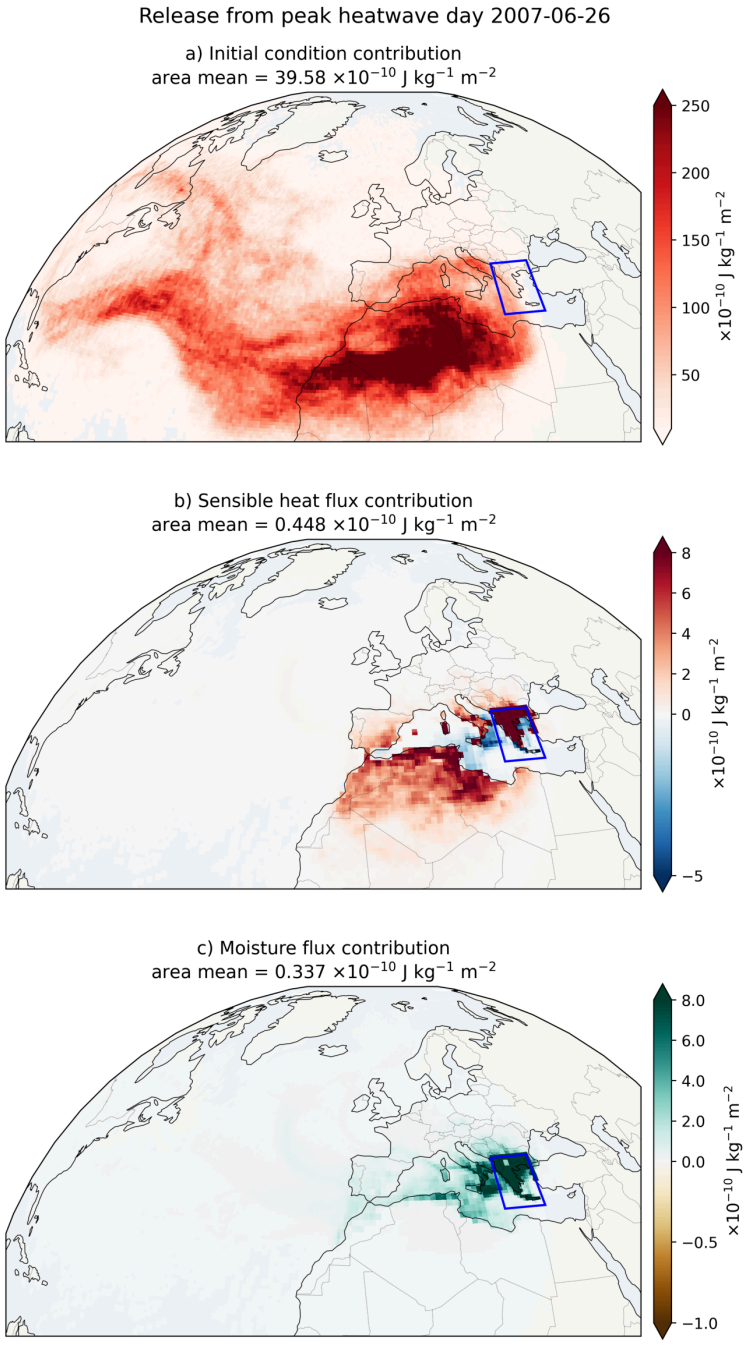


Figure 3. Components of the MSE reconstruction during 10 days backwards transport during the peak day of heatwave, averaged over all releases for that day. (a) Initial condition MSE contribution, i.e., initial-condition MSE at day -10 times the FLEXPART sensitivity to initial-conditions, summed over all vertical levels up to 25 km. (b) Sensible and (c) latent heat flux contributions, accumulated over the ten-day tracking period. All panels in J kg^{-1} m^{-3}, The blue box marks the receptor domain.

https://doi.org/10.5194/egusphere-2026-6583
Preprint. Discussion started: 17 November 2026
© Author(s) 2026. CC BY 4.0 License.

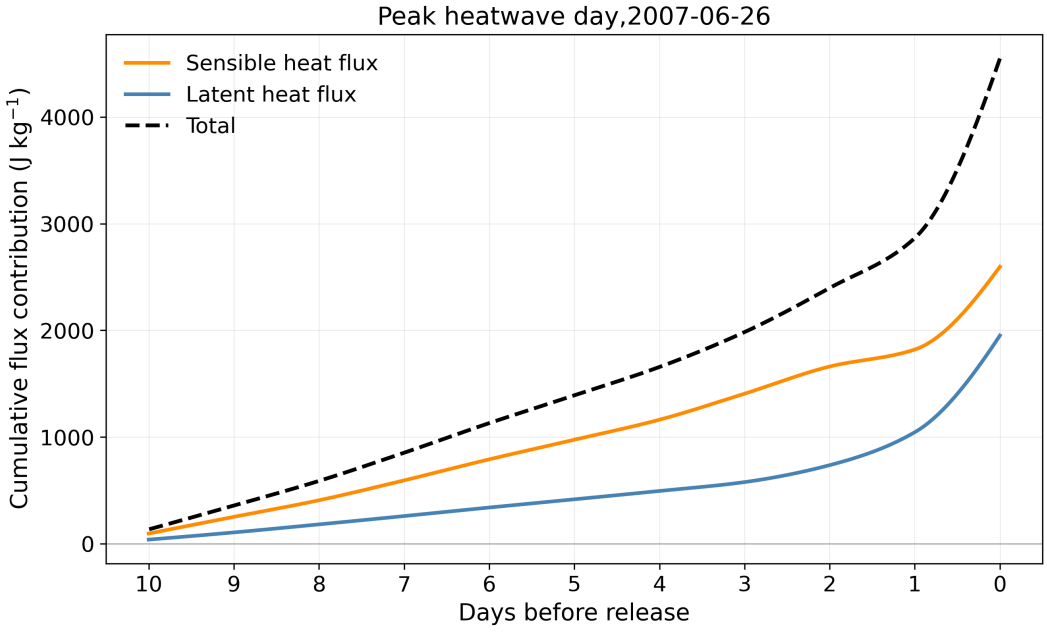


Figure 4. Sensible and latent heat flux contribution to the moist static energy for heatwave days occurring in year 2007, as a function of time along the ten-day backward pathway. Bars (left axis) show the mean contribution added on each individual day, solid lines (right axis) show the cumulative contribution from day 10 (trajectory origin) to day 0 (release). The dashed black line shows the combined sensible and latent total.

variability is reproduced quite well. Comparing the two curves statistically (Fig. 5b) gives a Pearson correlation of $r = 0.90$ ($p < 0.001$), which suggests that the framework reproduces many aspects of the day-to-day variability of the receptor MSE. The points lie close to, but consistently below, the 1:1 line, showing that the reconstructed values exceed the ERA5 values by about 3845 J kg^{-1} on average. Dividing this value by C_p expresses this as a temperature-equivalent offset of roughly 4 K, or 0.4 K day^{-1} over the ten-day backward period during the pathway. This bias is expected because three-dimensional radiative fluxes are not included. A neglected loss of 0.4 K day^{-1} is roughly consistent with clear-sky radiative cooling rates expected at the top of the ABL (Fildier et al., 2023a; Hartmann et al., 2022). The imperfect correlation between reconstructed and actual MSE is likely due to data assimilation increments of MSE during the tracking period. Variations in radiative cooling, as well as heating due to evaporation of falling hydrometeors – which is also neglected in our framework – might also contribute.

The most important result seen in Fig. 5a is the dominant role of the advection of the initial conditions, which makes up not only for most of the absolute values of MSE at the receptor but also drives the daily variability of MSE at the receptor. This is consistent with previous studies (Röthlisberger and Papritz, 2023; Mayer and Wirth, 2025). The sensible heat flux contribution (Fig 3b) concentrates over North Africa and Greece, whereas the latent heat flux contribution (Fig 3c) is confined to the Mediterranean Sea and wetter land areas west to the receptor. Quantitatively, the receptor region supplies the largest single share of the surface-flux contribution (36%), followed by North Africa (15%). The Balkans and Western Europe together

https://doi.org/10.5194/egusphere-2026-6583
Preprint. Discussion started: 17 November 2026
© Author(s) 2026. CC BY 4.0 License.

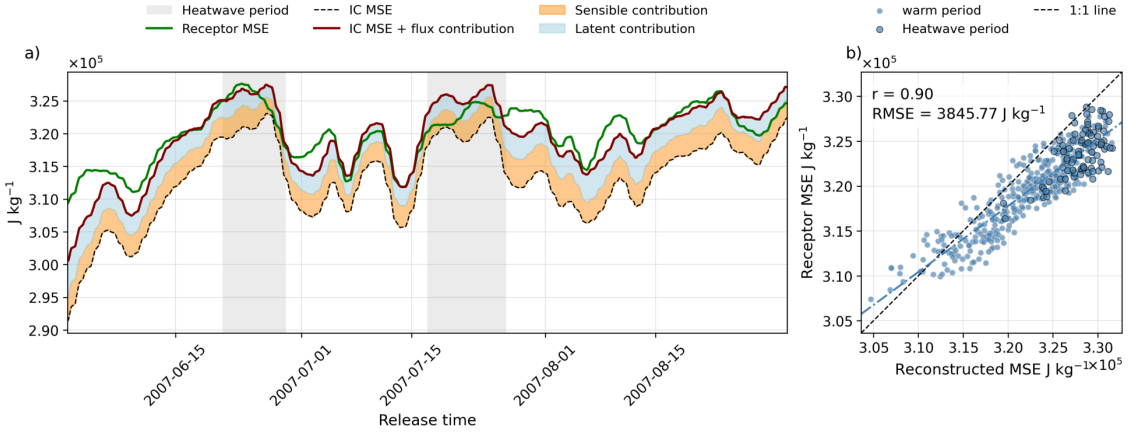


Figure 5. MSE budget closure for the 2007 Greek heatwave. (a) Time series of the initial-condition MSE (black dashed line), sensible heat flux contribution (orange shading), latent heat flux contribution (blue shading), total reconstructed MSE (maroon line), and ERA5 MSE for the receptor region (green line). Grey shading highlights the two detected heatwave periods. (b) Scatter plot of reconstructed versus ERA5 receptor MSE. Dark blue dots indicate data for the two detected heatwave days, light blue dots indicate all other data. The black dashed line shows the 1:1 relationship, and the blue dash-dotted line shows the linear fit.

contribute about 24%, and the Mediterranean about 9%. Region definitions as well as relative contributions for the 2007 and all other heat waves are shown in Fig. 7. Sensible heating accounts for 57.5% and latent heating for 42.5% of the total flux. The persistent anticyclonic ridge over the central and eastern Mediterranean (shown in Fig 8d) leads to the air mass transport northward across the Sahara, so the pathway crossed a region with very large sensible heat fluxes before reaching the receptor region that itself had strong sensible and latent heating. Remote Saharan sensible-heat uptake combined with local land-surface heating and evaporation are therefore the dominant flux contributions for this event.

3.2 Other Greek heatwaves

In order to put the result for the 2007 heatwaves into context, the same reconstruction framework is applied to the 10 other detected Greek heatwave events (Table 1). In every case it reproduces the day-to-day variability of the receptor MSE quite well, with correlations of $r = 0.85$–0.94 (all $p < 0.001$; Fig. S1 in the Supplement) and a systematic positive residual of the same sign and roughly the same magnitude as in the 2007 case. The attribution framework therefore behaves consistently across events of different intensity and duration and for different circulation pattern.

3.2.1 Differences in airmass transport for heatwave days and rest of summer days

Daily FLEXPART backward simulations were made throughout the summer for 7 years with heatwaves, allowing to analyse the differences in initial conditions and flux contributions between heatwave days and other summer days. On heatwave days, the MSE 10 days before the air mass arrival (initial conditions) is higher than on other summer days (see Fig. 6a). The largest

https://doi.org/10.5194/egusphere-2026-6583
Preprint. Discussion started: 17 November 2026
© Author(s) 2026. CC BY 4.0 License.

contribution to this comes from anomalous potential energy (gz), which is higher for every event, with the median being 5700 J kg^{-1} higher. Heatwave air therefore starts at higher altitudes than air arriving on other summer days. As the airmass descends towards the receptor, this potential energy is converted into enthalpy by adiabatic warming. For three events (1982, 1987 and 2021) the enthalpy (C_pT) is also higher for heatwaves airmasses 10 days before (4200–5700 J kg^{-1}). However, for the other four events, the initial enthalpy is almost the same as for other summer days (only slightly higher for heatwaves). The latent heat term (L_vq) differs only little (below 1000 J kg^{-1}) and its median is actually slightly lower for heatwave days as compared to other summer days. In absolute terms, enthalpy makes up most of the initial MSE (see Fig 6a) about 85 %), but the difference between heatwave and summer days is carried mainly by potential energy.

The comparison of surface-flux contributions along the transport pathways (Fig. 6b) shows that the sensible heat flux contribution tends to be slightly higher on heatwave days (median about 300 J kg^{-1} higher, compared with other summer days), but the two distributions overlap strongly. In contrast, a clear difference is found for the latent heat flux contribution, which is lower for heatwave days in every event (median -1350 J kg^{-1}, compared with about -100 J kg^{-1} on other summer days). Ordinary summer days therefore gain more moisture from the surface than heatwave days, while the sensible heating stays similar or slightly stronger.

On heatwave days, air masses come from further south ten days before arrival than on ordinary summer days ((Fig. S3 in the Supplement)). This is found for each event, with the sensitivity-weighted mean initial latitude shifting 10° further south on heatwave days than on other summer days of the same year. Events with a larger southward shift also tend to be associated with more air originating over Africa, whereas on other summer days more air originates over the North Atlantic or North America (shown in supplementary material Fig. S2).

Heatwave air masses therefore differ systematically from ordinary summer air mass. They start their ten-day journey with higher MSE, at higher altitudes and further south, over North Africa rather than the North Atlantic or North America (shown in Supplementary Fig. S3). During the transport, the sensible heat flux contribution is similar or slightly higher than on other summer days, while the latent heat flux contribution is actually substantially lower. This is consistent with more of the pathway lying over the dry Saharan region, where the surface adds sensible heat but little moisture.

In summary, the MSE anomaly of heatwave days is mostly due to higher potential energy 10 days back, in some cases with smaller contributions by initially higher enthalpy and surface sensible heat fluxes during transport. In contrast, lower latent heat fluxes during transport actually reduce the MSE anomalies compared to other summer days. The great importance of the advection of initial conditions is consistent with previous studies of Mayer and Wirth (2025); Röthlisberger and Papritz (2023); Schumacher et al. (2019). In addition to this, the above results highlights that air masses arriving on other summer days actually gain more energy (sum of sensible and latent heat) from the surface than heatwave air masses during the 10 days of transport. The MSE anomalies of heatwave days can therefore solely be attributed to the initial conditions, while the surface fluxes during transport reduce these anomalies. Our findings, suggesting a moderating role of land-atmosphere interactions during the 10 days of transport, differ from previous studies emphasizing the importance of these interactions for producing heat waves (Seneviratne et al., 2006), but they do not exclude that such interactions contributed to the initial anomaly before the tracking period.

https://doi.org/10.5194/egusphere-2026-6583
Preprint. Discussion started: 17 November 2026
© Author(s) 2026. CC BY 4.0 License.

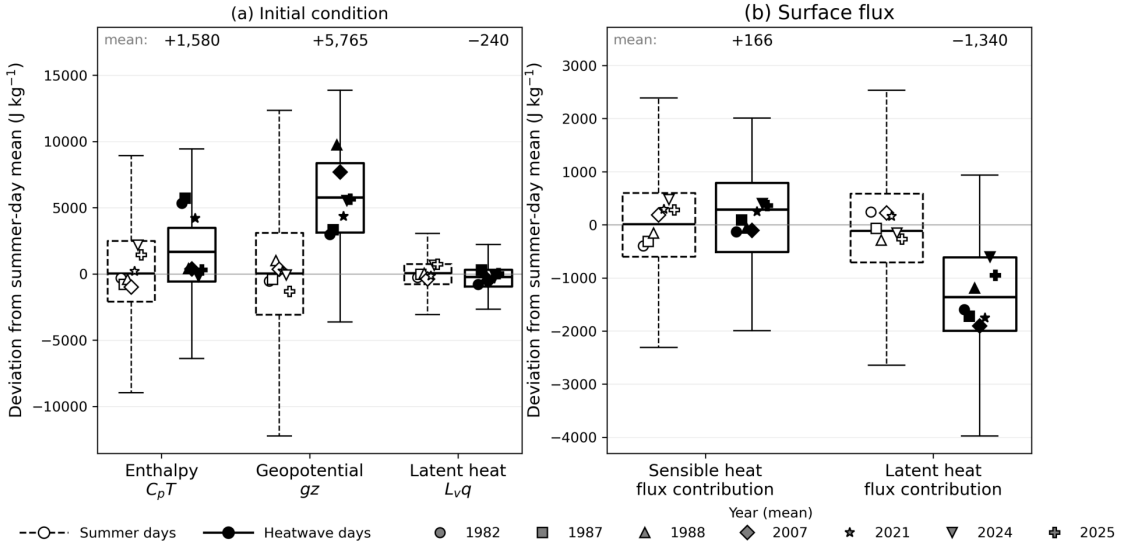


Figure 6. Comparison of heatwave days and summer days for all seven events combined ($n = 490$ heatwave and $n = 2475$ summer-day releases). a) Enthalpy (C_pT), geopotential (gz) and latent heat (L_vq) of the initial condition, ten days before arrival at the receptor region. b) Sensible and latent heat flux contributions gained along the ten-day transport. All values are deviations from the mean of all summer-day releases of the seven years. Boxes show the 25th to 75th percentiles with the median as a black line, whiskers extend to the most extreme values within 1.5 times the interquartile range, and outliers are not shown. Markers show the mean of each year, with the marker shape identifying the year. The mean difference between heatwave days and summer days (J kg^{-1}) is above each box. Summer days are shown with dashed boxes and open markers, heatwave days with solid boxes and filled markers.

Fig. 7 shows where the surface-flux contributions come from, for heatwave days (HD) and for ordinary summer days (SD). The total surface-flux contribution on heatwave days varies relatively little between events, from 5,303 J kg^{-1} in 2007 to 6,558 J kg^{-1} in 2024 (values above the HD bars), despite the marked differences in the synoptic setting and regional origin of these events discussed above. The energy the air mass gains from the surface is thus similar in all events, even though the regions supplying it shift from North Africa in the earlier events to continental Europe in the most recent ones. On average, it is about 1200 J kg^{-1} lower than on other summer days (Fig. 6b).

The comparison with other summer days shows what changes on heatwave days. On other summer days, the flux contribution comes mainly from the receptor region itself (31–35 %) and from the Balkans (16–19 %), with smaller shares from Western Europe, northeastern Europe and the North Atlantic, while North Africa supplies only 2 -5 %. On heatwave days, the local contribution stays about the same (31–39 %), but the remote sources change. North Africa supplies 26–31 % of the flux contribution in the events with the most southerly origins (1982, 1987 and 1988), about 21 % in 2021, 15 % in 2007, and only 6 -7 % in 2024 and 2025. In the first four years, this gain comes mainly at the expense of the Balkans, northeastern Europe and the North Atlantic. In 2024 and 2025, in contrast, the composition is close to that of other summer days, with the Balkans

https://doi.org/10.5194/egusphere-2026-6583
Preprint. Discussion started: 17 November 2026
© Author(s) 2026. CC BY 4.0 License.

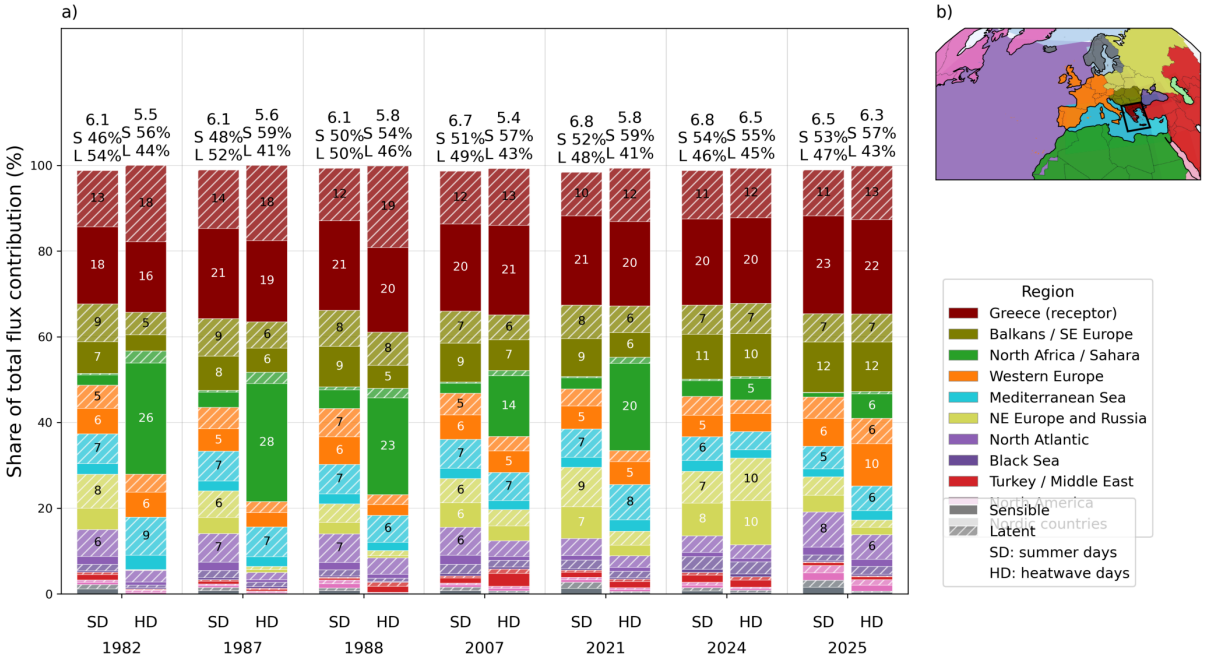


Figure 7. a) Regional shares of the surface-flux contribution for summer days (SD, left bars) and heatwave days (HD, right bars) in the seven events(1982–2025). Bars are split into sensible (solid) and latent (hatched) heating, and colours denote the source regions defined in the left geographic map. The number above each flux bar gives the mean surface-flux contribution per release in (kJ kg^{-1}), followed by its sensible (S) and latent (L) share in %.

(16–19 %), northeastern Europe (2024: 21 %) and Western Europe (2025: 16 %) supplying most of the remote contribution. This agrees with the small southward shift of the air mass in these two events (Fig. S3 in the Supplement).

The type of heating also differs between regions. Sensible heating dominates the flux contribution in all events, with 54–63 % (average of about 57 %), and is supplied mainly by dry continental land, in particular North Africa and the receptor region. Latent heating comes mainly from the Mediterranean, the Balkans and the wetter continental surfaces of Europe. Because the latent contribution is smaller on heatwave days compared to other summer days (Fig. 6b), the heatwave flux contribution is more dominated by sensible heating than that of other summer days. Maritime regions such as the Mediterranean Sea carry a large share of the air mass transport but contribute comparatively little to the flux contribution, because summer surface sensible heat fluxes are smaller over the sea and ocean than over land. For the Atlantic, the near-surface sensitivity is also small, because the air is mostly at higher altitudes far from the receptor. The receptor region supplies about one third of the flux contribution on both heatwave and other summer days, and on heatwave days this is split about equally between sensible and latent heating. This highlights the importance of local land-surface heating under anticyclonic subsidence and strong solar insolation.

https://doi.org/10.5194/egusphere-2026-6583
Preprint. Discussion started: 17 November 2026
© Author(s) 2026. CC BY 4.0 License.

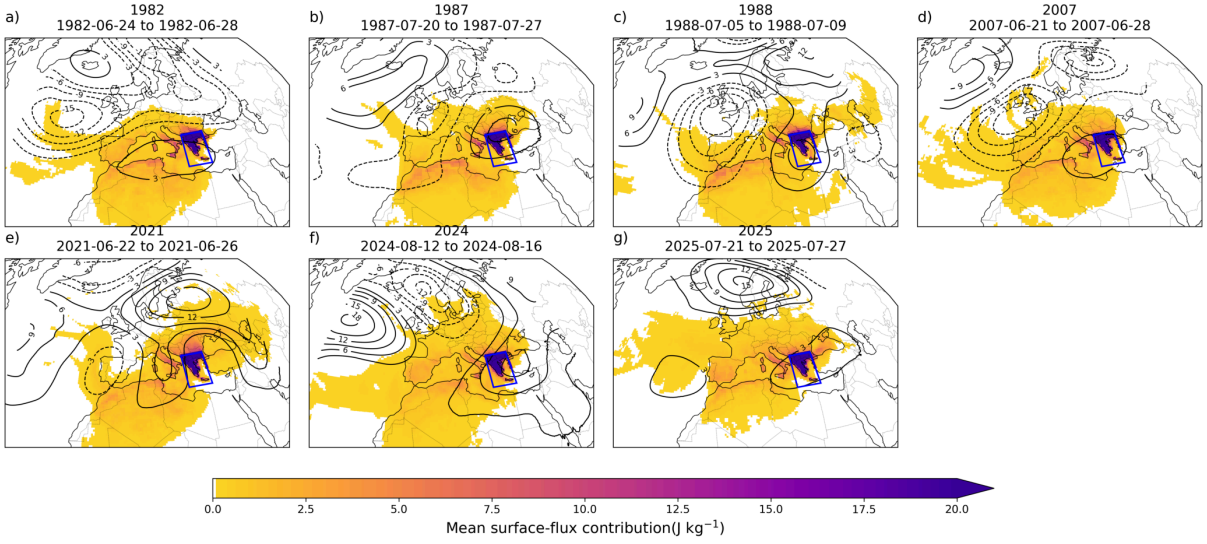


Figure 8. 500 hPa geopotential height anomalies (isolines; solid positive, dashed negative) and surface-flux contributions to receptor MSE (shading), both averaged over the same ten-day backward window preceding each event's strongest heatwave episode (window dates given above each panel). The blue box marks the Greece receptor domain.

The upper-level circulation that sets these pathways is shown in Fig. 8, which overlays the 500 hPa geopotential height anomaly, averaged over the transport window of each year's strongest heatwave episode, on the total surface-flux contribution. The events with southerly origins and a high North African share (1982 and 2007; Fig. 8a and d) are associated with a negative anomaly to the west, consistent with southerly flow ahead of an upper level trough. In 2025 (Fig. 8g), a positive anomaly lies over northern Europe in a Rex-block-like pattern, and the flux contribution comes mainly from continental Europe. In 2024 (Fig. 8f), a strong positive anomaly over the Atlantic and a negative anomaly over northeastern Europe point to northerly flow towards Greece, consistent with the northern origin of the air mass. The remaining events (1987, 1988 and 2021) show intermediate or mixed configurations, consistent with their regional flux contributions in Fig. 7.

4 Discussion and conclusions

A Lagrangian framework was developed that attributes the moist static energy (MSE) of a heatwave air mass to two physically distinct contributions: the energy the air mass already carried at the start of its transport pathway, considered here to be 10 days back in time, and the energy it subsequently acquired from surface sensible and latent heat fluxes. The framework couples ERA5 surface turbulent fluxes with the FLEXPART source–receptor relationship, and reconstructs the receptor MSE as the sum of the initial condition ten days upstream and the flux contribution accumulated along the way, allowing a detailed spatiotemporal attribution of that contribution. The new framework was demonstrated in detail for one heat wave in Greece, and applied to six others, as well as for the entire seven summer seasons.

https://doi.org/10.5194/egusphere-2026-6583
Preprint. Discussion started: 17 November 2026
© Author(s) 2026. CC BY 4.0 License.

Two aspects were addressed. The first was whether this reconstruction reproduces the observed day-to-day variability of receptor MSE. While the agreement is not perfect, there is a clear strong correlation in every event analysed ($r = 0.85$–0.94). There is also a systematic positive bias of the reconstructed compared to the actual receptor MSE. It seems likely that this bias can be attributed at least partly to radiative cooling of the air, which the framework currently does not account for.

The second aspect was whether the sensible and latent flux contributions, and their regional origin, can be quantified. To this end, it was found that the initial condition MSE contribution already accounts for most of the receptor MSE and varies three to five times more across events than the surface-flux contributions. This implies that, it sets most of the heatwave anomaly, ten days before arrival, the air mass already carries more energy and comes from further south.compared with ordinary summer days of the same summer year. This is consistent with previous studies (Mayer and Wirth, 2025; Röthlisberger and Papritz, 2023; Schumacher et al., 2019). The reason for the initial positive MSE anomaly of heatwave days compared to other summer days is mainly a positive potential energy anomaly, whereas enthalpy is only sometimes higher, and latent heat is similar to other summer days. An important finding of our study is that the surface fluxes during the 10-day transport actually reduce the initial MSE anomaly compared to other summer days. The reason for this is a negative anomaly in the uptake of latent heat compared to other summer days. Sensible heat uptake is slightly higher than on other summer days but cannot compensate the much larger negative anomalies in latent heating.

Long-range advection of initial conditions also dominates the day-to-day variability of the heatwave signal, while the surface fluxes only modulate it. Over the ten-day tracking period, the surface fluxes add comparatively similar amounts of MSE to the air mass in all seven heatwave cases, 5.4–6.5 kJ kg^{-1}, even though the advection differs strongly between them, in some events the fluxes are taken up mostly over North Africa, in others further north in Europe. Sensible heating provides 54–59 % of this (57 % on average) and latent heating the remaining 41–46 % (Fig. 7). On the other summer days of the same years, the fluxes add 6.1–6.8 kJ kg^{-1} (more as compared to heatwave days). The heatwave air mass gains somewhat less energy from the surface than air arriving on other summer days, by 0.2–1.2 kJ kg^{-1} 0.6 kJ kg^{-1} on average). This is due mainly to lower latent heating (Fig. 6b).

In all cases, the receptor region itself is the single largest source of the surface-flux contribution. Nevertheless, for the Greek heatwave episodes studied, the local land–atmosphere interactions (Seneviratne et al., 2006) seem to play a limited role compared with the surface fluxes outside Greece, taken together, and especially compared with the long-range advection of air that already carried high MSE ten days earlier.

Compared to previously used Lagrangian methods to examine the sources of heat (Schumacher et al., 2019; Zschenderlein et al., 2019, 2020), our new method has distinct advantages and disadvantages. Its advantage is that it can quantitatively attribute the moist static energy of an air mass to specific processes like the surface fluxes of sensible and latent heat occurring during the recent history of that air mass. Methods used by others (Schumacher et al., 2019; Zschenderlein et al., 2019) diagnose these fluxes indirectly from changes in thermodynamic quantities of the tracked air mass, which can lead to erroneous attribution because these quantities only reflect the net effect of different processes. Furthermore, thermodynamic changes along trajectories are inherently noisy, due to data assimilation, trajectory errors and subgrid-scale processes such as convection, which can cause large errors in fluxes diagnosed from air parcel properties. A disadvantage of our method is that it relies entirely on the

https://doi.org/10.5194/egusphere-2026-6583
Preprint. Discussion started: 17 November 2026
© Author(s) 2026. CC BY 4.0 License.

quality of the fluxes taken from the meteorological model. Errors in these fluxes will directly lead to corresponding errors in the process attribution. Regarding this aspect, the previously used methods are more robust, since the air mass thermodynamic quantities are continuously corrected by the assimilation of temperature and other observations and thus rely less on the quality of the forecast model. The new method currently also neglects MSE losses due to radiative cooling and therefore cannot discount the contributions of earlier MSE uptakes.

The initial condition is evaluated at a fixed ten-day horizon, so both the partitioning of its energy between enthalpy, latent energy and potential energy and the regions identified as its origin depend on this choice. The current study is mainly intended to demonstrate the potential of our attribution framework, which still has some limitations. However, extensions of this work could address these limitations directly. The air mass is currently coupled only to surface turbulent fluxes, so radiative heating and cooling along the pathway are not included. ERA5 provides radiative temperature tendencies on model levels, and since FLEXPART computes the source–receptor relation as a three-dimensional field, these could be coupled to it, which is left for future work. The evaporation of rain falling into the tracked air mass could be included using further fields from the ECMWF model. The ten-day tracking period could also be extended. Longer backward simulations, such as the 50-day tracking used by Vojta et al. (2024) for greenhouse gas fluxes, would produce smoother, less variable initial conditions, since particles are by then distributed over much of a hemisphere, and initial condition MSE contributions would be more representative of the seasonal hemispheric atmospheric MSE background. In contrast, more variability could then be attributed to the contribution of surface fluxes, for instance heat added in the tropics. Furthermore, especially after including radiative fluxes, discounting methods could be used, similar to those used in water studies (Sodemann et al., 2008), where the history of positive and negative flux contributions could be used to discount earlier heating contributions compared to more recent ones, which are less affected by compensating cooling after the warming.

As a further outlook, the new framework also offers a quantitative basis for improving the quite uncertain surface heat fluxes. Inverse modelling of the MSE budget based on the difference between reconstructed and actual MSE at the receptor could be used in the same way as inverse modelling based on modelled and observed greenhouse gas atmospheric mole fractions has been used to improve greenhouse gas fluxes (Thompson and Stohl, 2014). While the high spatiotemporal variability of heat and moisture fluxes makes this challenging, the prospect of better-constrained heat and moisture fluxes provides motivation to pursue it.

Beyond these methodological extensions, applying the framework to a larger set of events and to a wider range of regions would establish how the advective and surface flux contributions to heatwaves are partitioned climatologically, and how that partition shifts under drying soils and a warming mid-troposphere. Furthermore, the framework can also be used to investigate the energy budget of cold events or in a climatological setup.

Code availability. The codes used for the analysis, including the FLEXPART configuration, reconstruction of MSE and the scripts for figures 1 -7, is available at https://doi.org/10.5281/zenodo.23478028 ((Deshmukh, 2026a)).

https://doi.org/10.5194/egusphere-2026-6583
Preprint. Discussion started: 17 November 2026
© Author(s) 2026. CC BY 4.0 License.

Data availability. The processed model output on which the figures are based is available at https://doi.org/10.5281/zenodo.23405520 ((Deshmukh, 2026b)). FLEXPART v11.0 is available at https://www.flexpart.eu. ERA5 data are available from the Copernicus Climate Data Store (Hersbach et al., 2020).

Author contributions. VD designed the analysis, ran the simulations, wrote the code, produced the figures and wrote the manuscript. AS and MD contributed to the development of the methods and approaches, to the interpretation of the results, manuscript feedbacks and rewriting.

Competing interests. The authors declare that they have no competing interests

Acknowledgements. This work was funded by the European Commission through the Edu4ClimAte project (grant No. 101071247). ERA5 data used here is provided by the Copernicus Climate Change Service. The computations were performed on the JET computing cluster of the University of Vienna. university AI portal u:ai – KI-Software, Claude were used to help rephrase sentences in article, write and debug the Python code for the analysis and the figures. The author tested all code, checked the results against the original model output, and wrote all text and interpretations themselves.

https://doi.org/10.5194/egusphere-2026-6583
Preprint. Discussion started: 17 November 2026
© Author(s) 2026. CC BY 4.0 License.

References

Bakels, L., Tatsii, D., Tipka, A., Thompson, R., Dütsch, M., Blaschek, M., Seibert, P., Baier, K., Bucci, S., Cassiani, M., Eckhardt, S., Zwaaftink, C. G., Henne, S., Kaufmann, P., Lechner, V., Maurer, C., Mulder, M. D., Pisso, I., Plach, A., Subramanian, R., Vojta, M., and Stohl, A.: FLEXPART version 11: improved accuracy, efficiency, and flexibility, Geoscientific Model Development, 17, 7595–7627, https://doi.org/10.5194/gmd-17-7595-2024, 2024.

Davini, P., Corti, S., D'Andrea, F., Rivière, G., and von Hardenberg, J.: Improved Winter European Atmospheric Blocking Frequencies in High-Resolution Global Climate Simulations, Journal of Advances in Modeling Earth Systems, 9, 2615–2634, https://doi.org/10.1002/2017MS001082, 2017.

Deshmukh, V.: Surface flux contributions-codes, Zenodo [code], https://doi.org/10.5281/zenodo.23478028, 2026a.

Deshmukh, V.: Surface flux contributions-Data, Zenodo [data set], https://doi.org/10.5281/zenodo.23405520, 2026b.

Emanuel, K. A. and Živković Rothman, M.: Development and Evaluation of a Convection Scheme for Use in Climate Models, Journal of the Atmospheric Sciences, 56, 1766–1782, https://doi.org/10.1175/1520-0469(1999)056<1766:DAEOAC>2.0.CO;2, 1999.

Fildier, B., Muller, C., Pincus, R., and Fueglistaler, S.: How Moisture Shapes Low-Level Radiative Cooling in Subsidence Regimes, AGU Advances, 4, https://doi.org/10.1029/2023AV000880, 2023a.

Fildier, B., Muller, C., Pincus, R., and Fueglistaler, S.: How moisture shapes low–level radiative cooling in subsidence regimes, AGU Advances, 4, e2023AV000 880, https://doi.org/10.1029/2023AV000880, 2023b.

Fischer, E. M., Seneviratne, S. I., Vidale, P. L., Lüthi, D., and Schär, C.: Soil Moisture–Atmosphere Interactions during the 2003 European Summer Heat Wave, Journal of Climate, 20, 5081–5099, https://doi.org/10.1175/JCLI4288.1, 2007.

Founda, D. and Giannakopoulos, C.: The exceptionally hot summer of 2007 in Athens, Greece — A typical summer in the future climate?, Global and Planetary Change, 67, 227–236, https://doi.org/10.1016/j.gloplacha.2009.03.013, 2009.

Founda, D., Katavoutas, G., Pierros, F., and Mihalopoulos, N.: The Extreme Heat Wave of Summer 2021 in Athens (Greece): Cumulative Heat and Exposure to Heat Stress, Sustainability, 14, 7766, https://doi.org/10.3390/su14137766, 2022.

Hartmann, D. L., Dygert, B. D., Blossey, P. N., Fu, Q., and Sokol, A. B.: The Vertical Profile of Radiative Cooling and Lapse Rate in a Warming Climate, Journal of Climate, 35, 6253–6265, https://doi.org/10.1175/JCLI-D-21-0861.1, 2022.

Hersbach, H., Bell, B., Berrisford, P., Hirahara, S., Horányi, A., Muñoz-Sabater, J., Nicolas, J., Peubey, C., Radu, R., Schepers, D., Simmons, A., Soci, C., Abdalla, S., Abellan, X., Balsamo, G., Bechtold, P., Biavati, G., Bidlot, J., Bonavita, M., De Chiara, G., Dahlgren, P., Dee, D., Diamantakis, M., Dragani, R., Flemming, J., Forbes, R., Fuentes, M., Geer, A., Haimberger, L., Healy, S., Hogan, R. J., Hólm, E., Janisková, M., Keeley, S., Laloyaux, P., Lopez, P., Lupu, C., Radnoti, G., de Rosnay, P., Rozum, I., Vamborg, F., Villaume, S., and Thépaut, J.-N.: The ERA5 global reanalysis, Quarterly Journal of the Royal Meteorological Society, 146, 1999–2049, https://doi.org/10.1002/qj.3803, _eprint: https://onlinelibrary.wiley.com/doi/pdf/10.1002/qj.3803, 2020.

Katsouyanni, K., Trichopoulos, D., Zavitsanos, X., and Touloumi, G.: THE 1987 ATHENS HEATWAVE, The Lancet, 332, 573, https://doi.org/10.1016/S0140-6736(88)92699-2, 1988.

Kautz, L.-A., Martius, O., Pfahl, S., Pinto, J. G., Ramos, A. M., Sousa, P. M., and Woollings, T.: Atmospheric blocking and weather extremes over the Euro-Atlantic sector – a review, Weather and Climate Dynamics, 3, 305–336, https://doi.org/10.5194/wcd-3-305-2022, 2022.

Kuglitsch, F. G., Toreti, A., Xoplaki, E., Della-Marta, P. M., Zerefos, C. S., Türkeş, M., and Luterbacher, J.: Heat wave changes in the eastern Mediterranean since 1960, Geophysical Research Letters, 37, https://doi.org/10.1029/2009GL041841, 2010.

https://doi.org/10.5194/egusphere-2026-6583
Preprint. Discussion started: 17 November 2026
© Author(s) 2026. CC BY 4.0 License.

Lelieveld, J., Hadjinicolaou, P., Kostopoulou, E., Chenoweth, J., Maayar, M. E., Giannakopoulos, C., Hannides, C., Lange, M. A., Tanarhte, M., Tyrlis, E., and Xoplaki, E.: Climate change and impacts in the Eastern Mediterranean and the Middle East, Climatic Change, 114, 667–687, https://doi.org/10.1007/s10584-012-0418-4, 2012.

Läderach, A. and Sodemann, H.: A revised picture of the atmospheric moisture residence time, Geophysical Research Letters, 43, 924–933, https://doi.org/10.1002/2015GL067449, 2016.

Mayer, A. and Wirth, V.: Two different perspectives on heatwaves within the Lagrangian framework, Weather and Climate Dynamics, 6, 131–150, https://doi.org/10.5194/wcd-6-131-2025, 2025.

Miralles, D. G., Teuling, A. J., van Heerwaarden, C. C., and de Arellano, J. V.-G.: Mega-heatwave temperatures due to combined soil desiccation and atmospheric heat accumulation, Nature Geoscience, 7, 345–349, https://doi.org/10.1038/ngeo2141, 2014.

Perkins, S. E.: A review on the scientific understanding of heatwaves—Their measurement, driving mechanisms, and changes at the global scale, Atmospheric Research, 164-165, 242–267, https://doi.org/10.1016/j.atmosres.2015.05.014, 2015.

Röthlisberger, M. and Papritz, L.: Quantifying the physical processes leading to atmospheric hot extremes at a global scale, Nature Geoscience, 16, 210–216, https://doi.org/10.1038/s41561-023-01126-1, 2023.

Say, D., Manning, A. J., O'Doherty, S., Rigby, M., Young, D., and Grant, A.: Re-Evaluation of the UK's HFC-134a Emissions Inventory Based on Atmospheric Observations, Environmental Science & Technology, 50, 11 129–11 136, https://doi.org/10.1021/acs.est.6b03630, 2016.

Schumacher, D. L., Keune, J., van Heerwaarden, C. C., de Arellano, J. V.-G., Teuling, A. J., and Miralles, D. G.: Amplification of mega-heatwaves through heat torrents fuelled by upwind drought, Nature Geoscience, 12, 712–717, https://doi.org/10.1038/s41561-019-0431-6, 2019.

Seibert, P. and Frank, A.: Source-receptor matrix calculation with a Lagrangian particle dispersion model in backward mode, Atmospheric Chemistry and Physics, 4, 51–63, https://doi.org/10.5194/acp-4-51-2004, 2004.

Seneviratne, S. I., Lüthi, D., Litschi, M., and Schär, C.: Land–atmosphere coupling and climate change in Europe, Nature, 443, 205–209, https://doi.org/10.1038/nature05095, 2006.

Sodemann, H., Schwierz, C., and Wernli, H.: Interannual variability of Greenland winter precipitation sources: Lagrangian moisture diagnostic and North Atlantic Oscillation influence, Journal of Geophysical Research: Atmospheres, 113, https://doi.org/10.1029/2007JD008503, 2008.

Stefanon, M., D'Andrea, F., and Drobinski, P.: Heatwave classification over Europe and the Mediterranean region, Environmental Research Letters, 7, 014 023, https://doi.org/10.1088/1748-9326/7/1/014023, 2012.

Stohl, A. and James, P.: A Lagrangian Analysis of the Atmospheric Branch of the Global Water Cycle. Part I: Method Description, Validation, and Demonstration for the August 2002 Flooding in Central Europe, Journal of Hydrometeorology, 5, 656–678, https://doi.org/10.1175/1525-7541(2004)005<0656:ALAOTA>2.0.CO;2, 2004.

Stohl, A., Wernli, H., James, P., Bourqui, M., Forster, C., Liniger, M. A., Seibert, P., and Sprenger, M.: A New Perspective of Stratosphere–Troposphere Exchange, Bulletin of the American Meteorological Society, 84, 1565–1574, https://doi.org/10.1175/BAMS-84-11-1565, 2003.

Stohl, A., Seibert, P., Arduini, J., Eckhardt, S., Fraser, P., Greally, B. R., Lunder, C., Maione, M., Mühle, J., O'Doherty, S., Prinn, R. G., Reimann, S., Saito, T., Schmidbauer, N., Simmonds, P. G., Vollmer, M. K., Weiss, R. F., and Yokouchi, Y.: An analytical inversion method for determining regional and global emissions of greenhouse gases: Sensitivity studies and application to halocarbons, Atmospheric Chemistry and Physics, 9, 1597–1620, https://doi.org/10.5194/acp-9-1597-2009, 2009.

https://doi.org/10.5194/egusphere-2026-6583
Preprint. Discussion started: 17 November 2026
© Author(s) 2026. CC BY 4.0 License.



Thompson, R. L. and Stohl, A.: FLEXINVERT: an atmospheric Bayesian inversion framework for determining surface fluxes of trace species using an optimized grid, Geoscientific Model Development, 7, 2223–2242, https://doi.org/10.5194/gmd-7-2223-2014, 2014.

Vautard, R., Cattiaux, J., Happé, T., Singh, J., Bonnet, R., Cassou, C., Coumou, D., D'Andrea, F., Faranda, D., Fischer, E., Ribes, A., Sippel, S., and Yiou, P.: Heat extremes in Western Europe increasing faster than simulated due to atmospheric circulation trends, Nature Communications, 14, 6803, https://doi.org/10.1038/s41467-023-42143-3, 2023.

Vojta, M., Plach, A., Annadate, S., Park, S., Lee, G., Purohit, P., Lindl, F., Lan, X., Mühle, J., Thompson, R. L., and Stohl, A.: A global re-analysis of regionally resolved emissions and atmospheric mole fractions of SF 6 for the period 2005–2021, Atmospheric Chemistry and Physics, 24, 12 465–12 493, https://doi.org/10.5194/acp-24-12465-2024, 2024.

Witte, J. C., Douglass, A. R., da Silva, A., Torres, O., Levy, R., and Duncan, B. N.: NASA A-Train and Terra observations of the 2010 Russian wildfires, Atmospheric Chemistry and Physics, 11, 9287–9301, https://doi.org/10.5194/acp-11-9287-2011, 2011.

WMO: Climate Change: How Do We Know?, https://wmo.int/media/news/extreme-weather-new-norm, 2023.

Zittis, G., Hadjinicolaou, P., Almazroui, M., Bucchignani, E., Driouech, F., Rhaz, K. E., Kurnaz, L., Nikulin, G., Ntoumos, A., Ozturk, T., Proestos, Y., Stenchikov, G., Zaaboul, R., and Lelieveld, J.: Business-as-usual will lead to super and ultra-extreme heatwaves in the Middle East and North Africa, npj Climate and Atmospheric Science, 4, 20, https://doi.org/10.1038/s41612-021-00178-7, 2021.

Zschenderlein, P., Fink, A. H., Pfahl, S., and Wernli, H.: Processes determining heat waves across different European climates, Quarterly Journal of the Royal Meteorological Society, 145, 2973–2989, https://doi.org/https://doi.org/10.1002/qj.3599, 2019.

Zschenderlein, P., Pfahl, S., Wernli, H., and Fink, A. H.: A Lagrangian analysis of upper-tropospheric anticyclones associated with heat waves in Europe, Weather and Climate Dynamics, 1, 191–206, https://doi.org/10.5194/wcd-1-191-2020, 2020.